# Surface topography and free energy regulate osteogenesis of stem cells: effects of shape-controlled gold nanoparticles

Kamolrat Metavarayuth, Esteban Villarreal, Hui Wang, Qian Wang\*

#### **Key Words:**

biomaterials; gold nanoparticles; osteogenesis; stem cells; surface free energy

#### From the Contents

Introduction	165
Methods	166
Results	168
Discussion	171

#### **ABSTRACT**

The surface free energy of a biomaterial plays an important role in the early stages of cell-biomaterial interactions, profoundly influencing protein adsorption, interfacial water accessibility, and cell attachment on the biomaterial surface. Although multiple approaches have been developed to engineer the surface free energy of biomaterials, systematically tuning their surface free energy without altering other physicochemical properties remains challenging. In this study, we constructed an array of chemicallyequivalent surfaces with comparable apparent roughness through assembly of gold nanoparticles adopting various geometrically-distinct shapes but all capped with the same surface ligand, (1-hexadecyl)trimethylammonium chloride, on cell culture substrates. We found that bone marrow stem cells exhibited distinct osteogenic differentiation behaviours when interacting with different types of substrates comprising shape-controlled gold nanoparticles. Our results reveal that bone marrow stem cells are capable of sensing differences in the nanoscale topographical features, which underscores the role of the surface free energy of nanostructured biomaterials in regulating cell responses. The study was approved by Institutional Animal Care and Use Committee, School of Medicine, University of South Carolina.

Department of Chemistry and Biochemistry, University of South Carolina, Columbia, SC. USA

\*Corresponding author: Qian Wang, Wang263@mailbox.sc.edu.

http://doi.org/10.12336/ biomatertransl.2021.02.006

How to cite this article: Metavarayuth, K.; Villarreal, E.; Wang, H.; Wang Q. Surface topography and free energy regulate osteogenesis of stem cells: effects of shape-controlled gold nanoparticles. *Biomater Transl.* **2021**, *2*(2), 165-173.



#### Introduction

The interface between biomaterials and living tissues is a key structural factor dictating the cellular responses.1 In particular, tissue healing and/or regeneration processes are guided by the local surface curvature or topographical features of the cell surroundings, such as extracellular matrix and other neighbouring cells. Consequently, the surface topographical features of a biomaterial can profoundly influence cell fate determination, adhesion, polarisation, and migration.2 It is widely accepted that cells can sense their external environment and interact with biomaterials locally at the nanometre level.<sup>3,4</sup> Cell interactions with nanometric surfaces often result in either cytoskeletal organisation and protein orientation or protein unfolding, thus directing cellular functions.<sup>5</sup> Previous studies by our group have shown that plant virus nanoparticles with unique nanoscale surface features can accelerate the osteogenesis of stem

cells both in vitro and in vivo when incorporated in either two- or three-dimensional scaffolds.6-9 We hypothesised that the distinctive nanoscale arrangement of viral coat proteins is critical to the osteogenic inductivity of plant virus scaffolds, as similar nanoparticles without the orderly arrangement of coat protein lack the ability to improve the osteogenesis of stem cells.7 In addition, hydrogel containing a mutant plant virus featuring the nano-spacing tripeptide Arg-Gly-Asp, the most common peptide motif responsible for cell adhesion to the extracellular matrix, further enhanced bone regeneration of a calvarial defect in both normal and osteoporotic ovariectomised rat models. 10, 11 In another study, however, no difference in the differentiation of stem cells was observed among various substrates coated with spherical, rigid rod-shaped, or fibre-like viral nanoparticles.8 From the physicochemical point of view, the surface curvature, ligand coating, surface atomic

coordination, and surface free energy are all intimately tied to the geometric shapes of the nanoparticles, and a strong synergy may exist among the above-mentioned structural factors when dictating cell differentiation behaviours.

One characteristic of surface features that has been widely disregarded is the inherent difference in surface energy. The surface atoms are undercoordinated, possessing fewer nearest neighbours than the atoms in the bulk. 'Dangling bonds' exposed at a material's surface give rise to extra 'unsatisfied bond energy'.12 When biomaterials are implanted or come into contact with the biological environment, water interactions, protein adsorption, and cell attachment are governed by the intermolecular bonds at the material's surface or the surface energy of the material.<sup>12</sup> The initial adhesion of cells to biomaterials is key to the regulation of subsequent proliferation, differentiation, and ultimately tissue formation at the interface. 13, 14 Therefore, understanding how surface energy affects the interactions of a surface with the biological environment is of pivotal importance to the rational design of biomaterials with specifically-targeted functions.

Common techniques employed to optimise surface energy are: 1) surface treatment to alter chemical properties, i.e. surface functionalisation,<sup>15</sup> surface etching,<sup>16</sup> and plasma treatment;<sup>17</sup> 2) mechanical manipulation to modify roughness and/or topography;<sup>18</sup> and 3) controlling crystallographic structure.<sup>19</sup> Nakamura et al.<sup>20</sup> investigated the surface characteristics of various types of hydroxyapatite after sintering in different atmospheres. The processes led to materials with differences in surface energy and wettability. They found that increased surface energy and enhancement of wettability accelerated cell adhesion.<sup>20</sup>

Razafiarison et al.<sup>21</sup> constructed polydimethylsiloxane-based scaffolds and mechanically adjusted them within the stiffness range from 70 Pa–2.3 MPa by using a surface energy gradient, without influencing the bulk properties and collagen topography of the biomaterials. Their results indicated that the surface energy-driven ligand self-assembly could direct the mechanosensitivity of mesenchymal stem cells, resulting in changes in cell spreading and differentiation based on polydimethylsiloxane stiffness.<sup>21</sup>

Generally, altering the surface structures of a material often lead to modification of a series of properties, such as surface energy, chemical functionalities, and interfacial hydrophobicity, all of which will affect the way cells interact with the surface. One method that can be employed to optimise surface energy of a material while maintaining other surface features is to modify the crystallographic termination of the surface. Faghihi et al.22 demonstrated how three main classes of crystallographic facets of titanium, specifically (1010), (1120), and (0001) facets, influenced the differential response of fibroblast and preosteoblast cell lines. Their results show that cells recognise the atomic structure of a surface differently, leading to celltype-dependent adhesion. Preosteoblasts attached significantly more on Ti-(1120), while fibroblast adhesion was amplified on Ti-(1010).<sup>22</sup> This demonstrates that the three distinct facets of titanium substrates differ significantly in their capacity to serve as cell-adhesion substrates.

Gold nanoparticles (AuNPs) exhibit a unique set of properties ideal for widespread applications ranging from biomimetic materials, over printed electronics to electrochemical biosensors.<sup>23-28</sup> The surface free energy of AuNPs can be tuned by changing the nanoparticle shapes, altering the arrangement of Au atoms on different crystallographic facets.<sup>29</sup> Seed-mediated nanocrystal growth with the aid of structuredirecting surface-capping ligands provides a versatile approach to the synthesis of colloidal AuNPs with precisely-controlled sizes and shapes.30 In this study, we fabricated an array of chemically-equivalent and topographically-comparable surfaces by depositing shape-controlled AuNPs with different surface energies onto cell culture substrates, which allowed us to investigate the osteogenic differentiation of stem cells on these surfaces as a function of nanoscale surface energy.

#### Methods

#### Synthesis of different shapes of gold nanoparticles

CTAB-capped Au clusters were prepared by reducing gold(III) chloride trihydrate (HAuCl<sub>2</sub>) with sodium borohydride (NaBH<sub>2</sub>) in the presence of 1-hexadecyltrimethylammonium bromide (CTAB). Typically, 0.60 mL of ice-cold, freshly-prepared NaBH (10 mM, 99%, Sigma-Aldrich, St. Louis, MO, USA) were quickly injected into a solution composed of CTAB (10.00 mL, 0.10 M, > 98%, TCI America, Portland, OR, USA) and HAuCl<sub>4</sub> (0.25 mL, 10 mM, ACS grade, J.T. Baker, Phillipsburg, NJ, USA) under magnetic stirring (300 r/min). The solution was stirred for 2 minutes and then left undisturbed for 3 hours at 27°C. The CTAB-capped Au clusters were used to prepare ~10 nm Au seeds by injecting 2 mL of HAuCl (0.5 mM) into a mixture of 2 mL of 1-hexadecyl)trimethylammonium chloride (CTAC; 0.2 M, 96%, Alfa Aesar, Ward Hill, MA, USA), 1.5 mL of freshly-prepared L-ascorbic acid (AA, 0.1 M, 99.5+%, Sigma-Aldrich), and 50 µL of the CTAB-capped Au cluster solution. The solution was stirred for 1 minute and left undisturbed for 15 minutes, and then the Au seeds were collected by centrifugation at  $16,100 \times g$  for 30 minutes. The obtained Au seeds were washed with water through centrifugation redispersion cycles, and redispersed in 1 mL of 0.02 M CTAC. The Au seed solution was used for subsequent seed-mediated growth. The final concentration of AA in the growth solution and the addition rate of HAuCl, were varied to control the speed of reduction to generate different-shaped AuNPs. The composition of the growth solution mixture and the HAuCl, addition rate for each AuNP are listed in Table 1.

After an hour of mixing at 27°C, the growth solution mixture was left undisturbed for 10 minutes before AuNPs were collected by centrifugation at 16,100 × g for 10 minutes. The obtained AuNPs were washed with water through centrifugation–redispersion cycles, and redispersed in 0.86 mL of water. In order to prepare ~70 nm diameter CCNPs, the CCNPs (46 nm) obtained from the previous step were used as seeds for another cycle of growth by injecting 2 mL of 0.5 mM HAuCl<sub>4</sub> at 2 mL/h to a mixture of CTAC (2 mL, 0.1 M), AA (70  $\mu$ L, 0.1 M) and CCNP (46 nm) seeds (500  $\mu$ L). The solution was left undisturbed overnight at 27°C and the CCNPs were collected using the same centrifugation–redispersion method as other AuNPs.

Table 1. The composition of growth solution mixture and HAuCl, addition rate for each AuNP

AuNP	L-ascorbic acid	Au seed	0.1 M (1-hexadecyl)trimethylammonium chloride	0.5 mM HAuCl <sub>4</sub> (2 mL) addition rate
Quasi-spherical nanoparticles	0.01 M, 130 μL	10 μL	2 mL	2 mL/h using a syringe pump
Nanotrioctahedra	0.1 Μ, 100 μL	10 μL	2 mL	1 shot injection (stir simultaneously)
Porous nanoparticles	0.1 M, 10 μL	10 μL	2 mL	1 shot injection (no stir)
Concave nanocube	0.1 M, 130 μL	10 μL	2 mL	2 mL/h using a syringe
particles				pump

Note: AuNP: gold nanoparticle; HAuCl<sub>4</sub>: gold(III) chloride trihydrate.

#### Gold nanoparticle characterisation

The size distributions of double-washed AuNPs were measured using dynamic light scattering (Zetasizer Nano ZS, Malvern Instruments, Malvern, UK) without further dilution. For transmission electron microscopy (TEM) analysis, 7  $\mu L$  of double-washed AuNP solution was dropped onto a 100-mesh carbon-coated copper grid and allowed to dry in a fume hood for 30 minutes at room temperature before imaging with a Hitachi H8000 electron microscope (Hitachi, Tokyo, Japan). The optical extinction spectra of the nanoparticles were measured in aqueous colloidal suspensions at room temperature, using a Beckman Coulter Du 640 spectrophotometer (Beckman Coulter, Brea, CA, USA).

#### Fabrication of gold nanoparticle-coated substrates

Glass cover-slips cleaned by piranha solution were incubated with triple-washed AuNPs for 6 hours in a tissue culture hood. After 6 hours, excess AuNP solution was removed and the substrates were washed immediately with nanopure water 3 times before allowing them to dry under a tissue culture hood. The AuNP-coated substrates were sterilised with UV-light for 15 minutes before use for cell culture.

# Surface characterisation of gold nanoparticle-coated surfaces by atomic force microscopy

The surface morphology of AuNP-coated substrates was observed by atomic force microscopy (AFM; Nanoscope IIIA MultiMode AFM, Veeco, Plainview, NY, USA). After coating with nanoparticles, the substrates were dried with a stream of nitrogen gas before being mounted onto the AFM sample holder for imaging in the tapping mode.

#### Contact angle measurement

Nanopure water (1 mL) was dropped onto AuNP-coated substrates and the contact angle was measured for each substrate using a video contact angle system (VCA-Optima, AST products, Inc., Billerica, MA, USA).

#### Quartz crystal microbalance measurement

A homemade quartz crystal microbalance (QCM) was used to measure the mass of the deposited layer using a 9 MHz quartz electrode coated with Ag on both sides. The quartz electrode was submerged in a triple-washed AuNP sample overnight before thoroughly washing with nanopure water to remove loosely-bound AuNPs. The AuNP-coated quartz electrode was incubated with cell culture medium and rinsed with nanopure

water before the QCM frequency shifts were monitored using a universal frequency counter (Protek C3100, Protek Test & Measurement, Allendale, NJ, USA).

#### Bone marrow stem cell isolation and expansion

Primary bone marrow stem cells (BMSCs) were isolated from the bone marrow of young adult male Wistar rats (8 weeks old, 80g body weight; Harlan Sprague-Dawley Inc., Indianapolis, IN, USA). Rats were euthanized by CO<sub>2</sub> in the euthanasia chamber. Procedures were performed in accordance with the guidelines for animal experimentation of the Institutional Animal Care and Use Committee, School of Medicine, University of South Carolina. Cells were maintained in primary medium (Hyclone, Thermo Scientific, Waltham, MA, USA) supplemented with 10% fetal bovine serum (Atlanta Biologicals, Flowery Branch, GA, USA) and 1% penicillin-streptomycin-amphotericin B (MP Biomedicals, Irvine, CA, USA; containing 100 U/mL of penicillin, 1000 U/mL of streptomycin solution, 0.25 µg/mL of amphotericin B), cultured at 37°C in a CO<sub>2</sub> incubator with 95% air/5% CO, and passaged no more than seven times after isolation. To induce osteogenesis, primary medium was replaced with osteogenic medium consisting of primary medium supplemented with 10 mM sodium β-glycerophosphate (Sigma-Aldrich), 50 µg/mL L-ascorbic acid 2-phosphate (Sigma-Aldrich), and  $1 \times 10^{-8}$  M dexamethasone (Enzo Life Sciences, Farmingdale, NY, USA). Medium was replenished every 3-4 days.

#### Alkaline phosphatase activity

After 2 days of induction in osteogenic medium, number of the BMSCs seeded onto a gold-sputtered surface and different AuNP-coated substrates were determined by CellTiter Blue assay. Then 4% paraformaldehyde was added at room temperature to fix the cells for 15 minutes. After that alkaline phosphatase (ALP) activity was analysed by incubating the fixed cells with 1-Step p-nitrophenylphosphate solution (Thermo Fisher Scientific) for 15 minutes at room temperature. Then the reaction was stopped by adding 250  $\mu L$  of 2 N NaOH to the incubated solution that was transferred to a new microfuge tube. Absorbance at 405 nm of the mixture was measured and was normalised to the corresponding cell number. Three independent experiments were analysed for ALP activity. Uncoated glass substrates were used as control.

#### Alizarin red staining and quantification

After 5 days of induction in osteogenic medium, cells were

fixed by 4% paraformaldehyde as described above, then the fixed cells were incubated with 0.1% Alizarin red solution (Sigma-Aldrich) pH 4.1–4.5 for 30 minutes in the dark and washed with water (18.2  $M\Omega$ ) prior to imaging. An Olympus IX81 fluorescent microscope (Olympus, Tokyo, Japan) was used to capture the stained substrates images. To quantify the amount of dye on each substrate, the dye on each sample was extracted by rinsing the samples with 300  $\mu L$  of 0.1 N NaOH. The extracted dye solution was measure absorbance at 548 nm wavelength. The measured absorbance from each sample was normalised to the corresponding cell number from CellTiter Blue assay. Three independent experiments were analysed for Alizarin red staining and quantification.

#### Statistical analysis

All data are expressed as mean  $\pm$  standard deviation (SD). Statistical analysis was performed by analysis of variance with

Tukey's multiple comparisons tests using GraphPad Prism 5 (GraphPad Software, San Diego, CA, USA). A value of P < 0.05 was considered to be statistically.

#### Results

## Shape-controlled synthesis of gold quasi-spherical, trisoctahedral, porous, and concave cubic nanoparticles

AuNPs of different shapes were synthesised through seed-mediated colloidal nanocrystal growth processes under kinetically-controlled conditions.<sup>31-33</sup> By controlling the reduction rate of Au<sup>3+</sup> to Au<sup>0</sup>, AuNPs with different shapes but the same surface chemical properties were obtained (**Figure 1**). Upon depositing these AuNPs onto cell culture substrates, the nanoscale surface energy could be fine-tuned while maintaining similar chemical composition and surface topography.

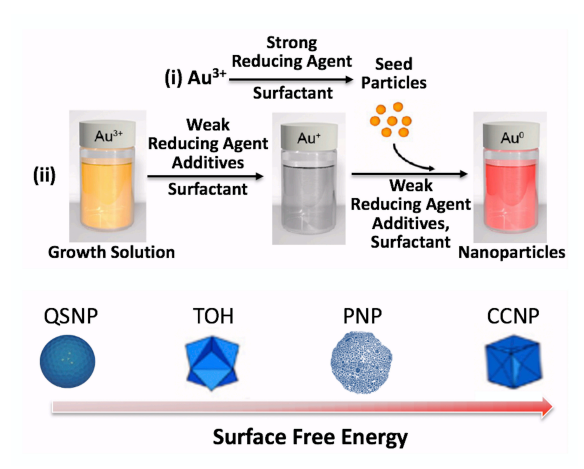


**Figure 1.** Seed-mediated synthesis of AuNPs with different shapes. Seed particles were first prepared by reduction of Au<sup>3+</sup> in a strong reducing agent as the first step. Then the Au<sup>3+</sup> growth solution was reduced in weak reducing agent and surfactant to Au<sup>+</sup> which was kinetically controlled to grow on seed particles from the first step into gold nanoparticles with different shapes. Slower reduction rates produced AuNPs that were more stable or had lower surface energies such as quasi-nanospheres enclosed by {111} and {100} facets, while faster reaction rates produced high index faceting Au QSNPs with higher surface energies, such as TOH, PNPs, and CCNPs.<sup>31, 32</sup> AuNPs: gold nanoparticles; CCNPs: concave nanocube particles; PNPs: porous nanoparticles; QSNPs: quasi-spherical nanoparticles; TOH: nanotrioctahedra.

TEM images of the four AuNPs show their morphology as quasi-spherical nanoparticles (QSNPs), nanotrioctahedra (TOH), porous nanoparticles (PNPs), or concave nanocube particles (CCNPs) (Figure 2A). Despite their geometricallydistinct shapes, the as-synthesised AuNPs exhibited similar particle sizes in the range of 80-100 nm as revealed by TEM images (Figure 2B). The mean sizes and the size distribution profiles of the AuNPs obtained from TEM were in excellent agreement with the hydrodynamic sizes quantified by dynamic light scattering (Figure 2C). Localised surface plasmon resonance is a distinct optical feature of AuNPs.34 As the particle shape varied, the characteristic plasmon resonance peak of the colloidal AuNPs shifted in the optical extinction spectra following the wavelength order of QSNPs < TOH < PNPs < CCNPs (Figure 2D), which was consistent with previous reports.<sup>32, 35</sup> Detailed structure–property relationships underpinning the shape-dependent plasmonic characteristics of these AuNPs have been reported in previous publications.<sup>31,32</sup>

### Fabrication of gold nanoparticle-coated substrates for stem cell differentiation studies

AuNPs with various shapes were deposited onto 'piranha'-treated glass cover slips. Owing to the positively-charged quaternary amine functional groups of CTAC and the negatively-charged surfaces of the 'piranha'-treated coverslips, the AuNPs were readily adsorbed onto the glass surface through electrostatic interactions (**Figure 3A**). The presence of AuNPs on the glass surface was confirmed by AFM (**Figure 3B**). The AFM images show similar coverage for all AuNP-coated substrates, which was approximately 40–50% for each substrate.

It is widely accepted that surface roughness is one of the major factors influencing cell responses, in particular stem cell differentiation.<sup>2</sup> Consequently the AuNP-coated substrates were analysed in terms of root mean square (Ra) roughness from images collected by AFM (**Figure 3C**). The Ra result revealed no significant difference in microscale roughness

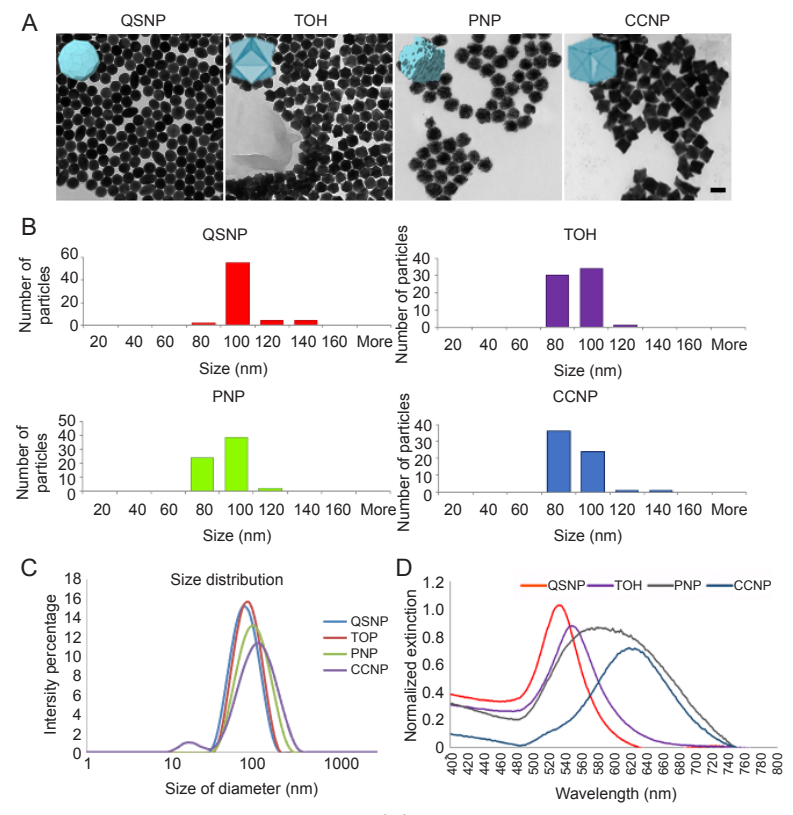


**Figure 2.** Characterisation of different-shaped AuNPs. (A) Transmission electron microscopic images of different-shaped AuNPs. The images show that AuNPs were similar in size and monodisperse in term of shape. Scale bar: 100 nm. (B) Particle size analysis of images obtained by transmission electron microscopy. AuNPs: gold nanoparticles; CCNPs: concave nanocube particles; PNPs: porous nanoparticles; QSNPs: quasi-spherical nanoparticles; TOH: nanotrioctahedra. (C) Size distribution of the different-shaped AuNPs analysed by dynamic light scattering. The results of dynamic light scattering showed a monodisperse peak of each shape of AuNPs with similar diameter, approximately 90 nm. (D) Optical extinction spectra of AuNPs reflecting differences in localised surface plasmon resonance.

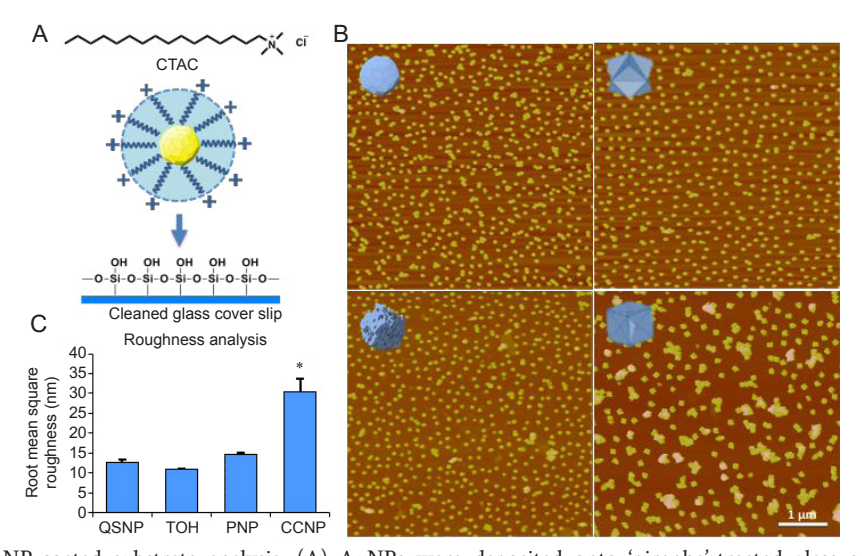


**Figure 3.** AuNP-coated substrate analysis. (A) AuNPs were deposited onto 'piranha'-treated glass cover-slips by electrostatic interaction between positively-charged quaternary amine function groups on AuNP ligands and negatively-charged 'piranha'-treated glass cover-slips. (B) Atomic force microscopic images show the different shapes of AuNP-coated substrates. The AuNP-coated glass cover-slips exhibited similar coverage of AuNPs on the substrate which was approximately 40–50%. (C) Root mean square (Ra) roughness from data collected from atomic force microscopic images. The Ra result revealed no significant difference in microscale roughness among QSNP-, TOH-, and PNP-coated substrates. CCNP-coated substrates showed significantly higher roughness compared to the other surfaces. Data are expressed as mean  $\pm$  SD. \*P < 0.05 based on one-way analysis of variance. AuNPs: gold nanoparticles; CCNPs: concave nanocube particles; CTAC: (1-hexadecyl)trimethylammonium chloride; PNPs: porous nanoparticles; QSNPs: quasi-spherical nanoparticles; TOH: nanotrioctahedra.

among substrates coated with QSNPs, TOH, and PNPs. Notably, CCNP-coated substrates showed significantly higher roughness than the other surfaces probably because the CCNPs tend to cluster together and form bigger and taller islands on the surface.

To explore the surface energy of the AuNP-coated substrates, the substrates were subjected to contact angle measurements and a gold sputtered surface was used as the benchmark material for comparison. Contact angle measurement results demonstrated that all AuNP-coated surfaces were more hydrophobic than an uncoated glass surface, as evidenced by the higher contact angle value of gold-containing surfaces compared to a bare glass surface (**Figure 4**). Among the AuNP-coated surfaces, QSNP was the most hydrophilic surface followed by gold-sputtered surface, CCNP-, TOH-, and PNP-coated substrates respectively.

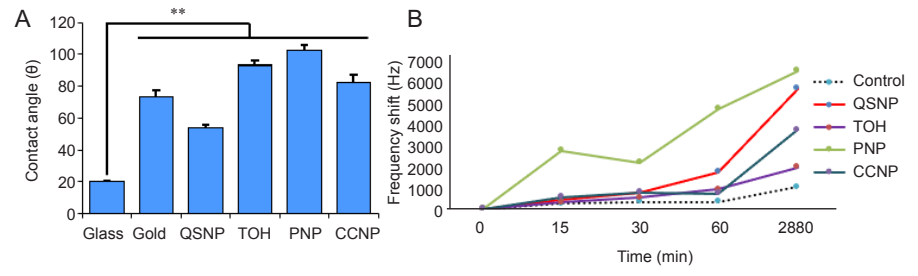


**Figure 4.** AuNP-coated substrate characterisation by contact angle measurement and QCM measurement. (A) AuNP-coated surfaces exhibit higher contact angles compared to an uncoated glass surface. QSNP is the most hydrophilic AuNP-coated surface, followed by gold sputtered surface, TOH-, CCNP-, and PNP-coated substrates respectively. (B) Frequency shifts measured by QCM after incubation of the AuNP-coated QCM probe with cell culture medium. Gold sputtered quartz probe was used as control. Data are expressed as mean ( $\pm$  SD). \*\* $P \le 0.01$  based on one-way analysis of variance. AuNPs: gold nanoparticles; CCNPs: concave nanocube particles; PNPs: porous nanoparticles; QCM: quartz crystal microbalance; QSNPs: quasi-spherical nanoparticles; TOH: nanotrioctahedra.

It is generally accepted that hydrophobic surfaces adsorb more proteins than hydrophilic surfaces. <sup>36, 37</sup> Therefore, we postulated that the higher energy surfaces which are hydrophobic (PNP and TOH) would exhibit higher protein adsorption. A hydrophobic surface allows interaction with hydrophobic domains and residues in the protein, a process which is assisted by an entropy gain during the subsequent release of unfavourably organised water at the surface.<sup>38</sup> QCM experiments showed that upon incubation with cell culture medium, the frequency of a QCM probe coated with PNP-AuNPs shifted rapidly, with an almost 3 kHz increase in frequency at 15 minutes of incubation observed for a PNP-coated QCM probe. On the other hand, other AuNPcoated QCM probes showed slight increases in frequency of less than 2 kHz even after incubation in cell culture medium for 1 hour. After 48 hours incubation, PNP-AuNPs absorbed the most mass, followed by QSNP, CCNP, TOH and gold-sputtered surfaces respectively. It is possible that the high porosity of the PNP-AuNPs resulted in a high surface area which led to greater adsorption of molecules onto the PNP-coated surface at every time-point measured. There was no significant difference in protein adsorption on QSNP, TOH and CCNP. This implies that the difference in surface energy across the three AuNP substrates may have little influence on protein adsorption at the incubation times studied. Deng et al.<sup>39</sup> reported that the shape of nanoparticles affected protein corona formation. For instance, spherical titanium dioxide NPs bind proteins that are not found on rod-like particles. This could explain the lack of correlation between surface energy and protein binding at the time-points observed in this study.

# Osteogenesis of rat bone marrow stem cells on substrates coated with different shapes of gold nanoparticle

To investigate the effect of differences in surface energy,

introduced by the different shapes of AuNPs, on cell differentiation, rat BMSCs were cultured on the panel of AuNPcoated substrates; QSNP, TOH, PNP, CCNP, and small cluster gold-sputtered surface. ALP, an early marker of osteogenesis, 40,41 was analysed in cells cultured on different AuNP substrates on day 2 and the results showed significantly higher enzyme activity in cells cultured on the QSNP-coated substrate which exhibited the lowest surface energy (Figure 5). Even though most studies analyse ALP activity on day 7 and later, in some studies higher levels of ALP activity have been observed earlier than day 7 and the elevated ALP level continues to increase from 7–14 days. 42,43 In addition, we previously observed significantly higher ALP activity which correlated with accelerated osteogenesis in BMSCs cultured in a three-dimensional scaffold of PEGgrafted hydrogel from days 3-7.44 We anticipated even faster cell differentiation in a two-dimensional culture environment; therefore, in this study we started assessing ALP activity from day 2. Similarly, studies often analyse Alizarin red S staining and measure calcium deposition later in the study, usually after 7-14 days. However, based on our previous studies with BMSCs as well as many previous reports, differentiation of BMSCs varies dramatically under the influence of many factors such as passage number, plating density and culture conditions. 45, 46 In our previous study, we observed formation of cell nodules which were positively-stained for calcium mineralisation as early as day 2 after osteoinduction when the cells were cultured on appropriate substrates. This suggests that it is possible to observe early osteogenic differentiation under the culture conditions and method of obtaining primary cells we routinely utilise in our studies. As a result, positive staining of cells by Alizarin red S, resulting in the deep red colour indicating calcium deposition in large cell nodules, was clearly observed in the cells cultured on QSNP and TOH as early as

day 5 after osteoinduction, whereas no staining was observed on gold-sputtered and PNP substrates (**Figure 6**). The Alizarin red S staining result confirms calcium mineralisation of cells on the two substrates. Notably, cells on CCNP substrate only formed small nodules that were also stained with Alizarin red

S. When the dye was dissolved and quantified by ultraviolet-visible spectrometry at 548 nm, the normalised absorbance of dye dissolved from cell nodules on QSNP followed by those on TOH substrates indicated higher calcium mineralisation on these two substrates than on other substrates.

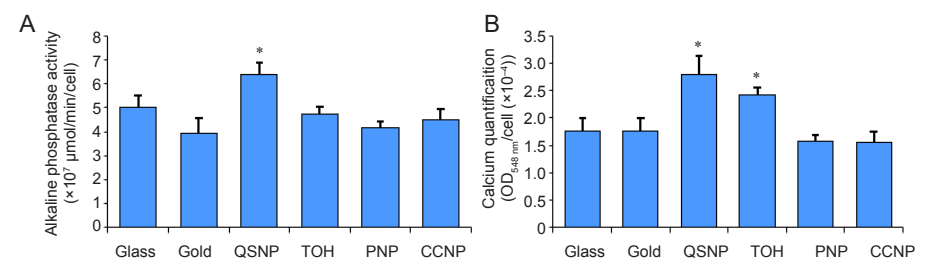


**Figure 5.** Cytochemical analysis of the osteogenic differentiation process of rat bone marrow stem cells on control glass, gold-sputtered substrates, and gold nanoparticle-coated substrates at day 2 after incubated in osteogenic media. (A) Alkaline phosphatase activity of cells cultured on different substrates. (B) Optical density at 548 nm of solubilised Alizarin red S staining normalised to cell number indicates the relative deposited calcium quantity at day 5. The mineralisation of cells on QSNP and TOH substrates was significantly higher than that of control glass, gold-sputtered, PNP and CCNP substrates. Data are expressed as mean  $\pm$  SD (n = 3). \*P < 0.05 (one-way analysis of variance followed by multiple comparisons). CCNPs: concave nanocube particles; PNPs: porous nanoparticles; QSNPs: quasi-spherical nanoparticles; TOH: nanotrioctahedra.

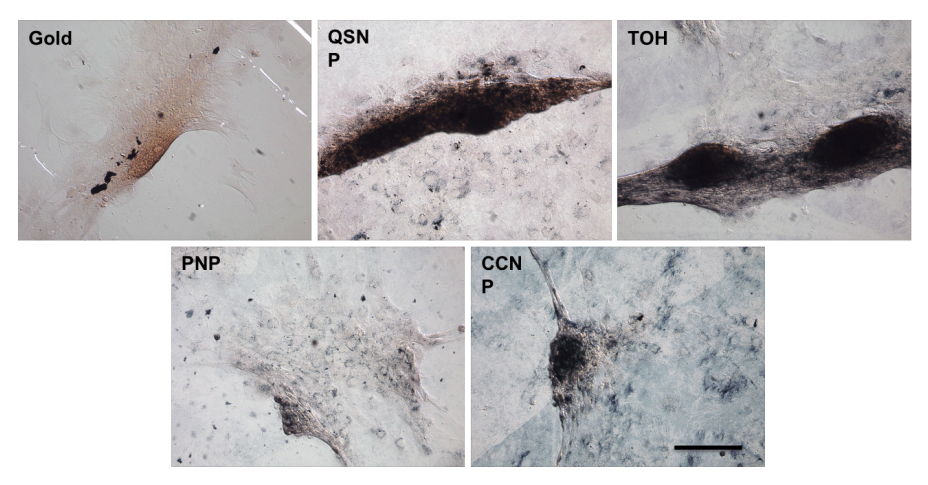


**Figure 6.** Micrographic images of bone marrow stem cells stained with lizarin red S staining of each sample at day 5. Cells on QSNP and TOH substrates are obviously stained for calcium deposition, as illustrated by the deep red colour for calcium of large cell nodules, whereas much weaker staining was observed on gold-sputtered and PNP-coated substrates. The Alizarin red S staining confirms calcium mineralisation of cells on the two substrates. Notably, cells on CCNP substrate only formed small nodules that were also stained with Alizarin red S. Scale bar: 200 μm. CCNP: concave nanocube particle; PNP: porous nanoparticle; QSNP: quasi-spherical nanoparticle; TOH: nanotrioctahedra.

#### Discussion

In general terms, researchers have often reported that surfaces with high surface energy or wettability promote cell adhesion, while low-energy surfaces are not supportive of cell attachment and spreading. <sup>47-52</sup> It has long been recognised that a cell's ability to adhere onto a surface plays a significant role in osteoblast differentiation. Specifically, BMSCs tend to differentiate into osteoblasts when they are cultured on surfaces that permit cell spreading, while those whose spreading is limited become adipocytes. The QSNP surface, which was shown to promote osteogenic differentiation, has a contact angle close to 65°. This result is consistent with a number of studies that reported that the ideal contact angle for best directing cell proliferation and behaviour is around 60°-70°. <sup>51-53</sup> While it is clear that

the nanoscale surface energy of these AuNPs relates to the observed phenomenon, other features such as the surface curvature, ligand coating, and surface atomic coordination, which are all interconnected to the nanoparticle shapes, most likely also contribute to the cell–material interaction and lead to the osteogenesis of stem cells.

Chemically-equivalent shape-controlled AuNPs were successfully synthesised by controlling the rate of reduction during the growth process of seed-mediated AuNP synthesis. The developed procedure was employed to prepare four different-shaped AuNPs: QSNPs, TOH, PNPs and CCNPs. The synthesised AuNPs contained distinct dominant facets leading to dissimilarities in surface energy pertaining to each type of AuNP. Upon depositing the AuNPs onto the cell culture

surface, an array of cell culture substrates exhibiting a range of surface energies with comparable chemistry and topography were generated, as evidenced by TEM, dynamic light scattering, contact angle, and AFM characterisations. These surfaces were employed to investigate cellular responses, in particular osteogenic differentiation of mesenchymal stem cells as a function of surface energy. QCM results demonstrated that protein adsorption onto these AuNP-coated surfaces varied based on the shape of AuNPs present on the substrate surface. Corresponding to the dissimilarity in protein adsorption, the combined results from ALP and calcium mineralisation assays suggested that mesenchymal stem cell differentiation on QSNP followed by TOH were enhanced relative to cells cultured on PNP, CCNP, small cluster gold sputter-coated, and glass control substrates. These results suggested that cells can sense the difference in surface energy within the controlled chemistry and topography milieu and uniquely respond to the change in their environment.

Further investigation of surface energy-induced differentiation is necessary for a better understanding of how surface energy provided by distinctly-shaped AuNPs affects protein conformational change, protein absorption, cell-material interaction, and ultimately cell differentiation. Additionally, a continued study can be extended to the investigation of other well-defined materials with surface energy manipulability on the cellular responses in both two- and three-dimensional models. Ultimately, it will be very fruitful to apply our discovery to other synthetic substrates employed in clinical tissue engineering applications.

#### **Author contributions**

Conceptualisation, methodology, project administration, funding acquisition: HW, QW; data generation and study design: MK, EV; original draft: MK; data curation, investigation and validation: MK, HW, QW; manuscript review & editing: MK, HW, QW. All authors approved the final version of this manuscript.

#### Financial support

The study was supported by National Science Foundation (NSF) and South Carolina Experimental Program to Stimulate Competitive Research and Institutional Development Awards (SC EPSCoR/IDeA) Program under NSF Award #OIA-1655740. The views, perspective, and content do not necessarily represent the official views of the SC EPSCoR/IDeA Program nor those of the NSF.

#### Acknowledgement

#### None

#### Conflicts of interest statement

The authors declare no competing financial interest.

Editor note: Qian Wang is an Editorial Board member of Biomaterials Translational.

The article was subject to the journal's standard procedures, with peer review handled independently of this Editorial Board Member and their research groups.

#### Data sharing statement

This is an open access journal, and articles are distributed under the terms of the Creative Commons Attribution-NonCommercial-ShareAlike 4.0 License, which allows others to remix, tweak, and build upon the work noncommercially, as long as appropriate credit is given and the new creations are licensed under the identical terms.

- Higuchi, A.; Ling, Q. D.; Chang, Y.; Hsu, S. T.; Umezawa, A. Physical cues of biomaterials guide stem cell differentiation fate. *Chem Rev.* 2013, 113, 3297-3328.
- Metavarayuth, K.; Sitasuwan, P.; Zhao, X.; Lin, Y.; Wang, Q. Influence of surface topographical cues on the differentiation of mesenchymal stem cells in vitro. ACS Biomater Sci Eng. 2016, 2, 142-151.

 Badami, A. S.; Kreke, M. R.; Thompson, M. S.; Riffle, J. S.; Goldstein, A. S. Effect of fiber diameter on spreading, proliferation, and differentiation of osteoblastic cells on electrospun poly(lactic acid) substrates. *Biomaterials.* 2006, 27, 596-606.

- Miller, D. C.; Thapa, A.; Haberstroh, K. M.; Webster, T. J. Endothelial and vascular smooth muscle cell function on poly(lactic-co-glycolic acid) with nano-structured surface features. *Biomaterials*. 2004, 25, 53-61.
- Rahmati, M.; Silva, E. A.; Reseland, J. E.; C, A. H.; Haugen, H. J. Biological responses to physicochemical properties of biomaterial surface. *Chem Soc Rev.* 2020, 49, 5178-5224.
- Kaur, G.; Valarmathi, M. T.; Potts, J. D.; Wang, Q. The promotion of osteoblastic differentiation of rat bone marrow stromal cells by a polyvalent plant mosaic virus. *Biomaterials*. 2008, 29, 4074-4081.
- Metavarayuth, K.; Maturavongsadit, P.; Chen, X.; Sitasuwan, P.; Lu, L.; Su, J.; Wang, Q. Nanotopographical cues mediate osteogenesis of stem cells on virus substrates through BMP-2 intermediate. *Nano Lett.* 2019, 19, 8372-8380.
- Metavarayuth, K.; Sitasuwan, P.; Luckanagul, J. A.; Feng, S.; Wang, Q. Virus nanoparticles mediated osteogenic differentiation of bone derived mesenchymal stem cells. *Adv Sci (Weinh)*. 2015, 2, 1500026.
- Sitasuwan, P.; Lee, L. A.; Bo, P.; Davis, E. N.; Lin, Y.; Wang, Q. A plant virus substrate induces early upregulation of BMP2 for rapid bone formation. *Integr Biol (Camb).* 2012, 4, 651-660.
- Yuan, J.; Maturavongsadit, P.; Zhou, Z.; Lv, B.; Lin, Y.; Yang, J.;
  Luckanagul, J. Hyaluronic acid-based hydrogels with tobacco mosaic virus containing cell adhesive peptide induce bone repair in normal and osteoporotic rats. *Biomater Transl.* 2020, 1, 89-98.
- Maturavongsadit, P.; Luckanagul, J. A.; Metavarayuth, K.; Zhao, X.; Chen, L.; Lin, Y.; Wang, Q. Promotion of in vitro chondrogenesis of mesenchymal stem cells using in situ hyaluronic hydrogel functionalized with rod-like viral nanoparticles. *Biomacromolecules*. 2016, 17, 1930-1938.
- Gentleman, M. M.; Gentleman, E. The role of surface free energy in osteoblast-biomaterial interactions. *Int Mater Rev.* 2014, 59, 417-429.
- Yang, D.; Lü, X.; Hong, Y.; Xi, T.; Zhang, D. The molecular mechanism of mediation of adsorbed serum proteins to endothelial cells adhesion and growth on biomaterials. *Biomaterials*. 2013, 34, 5747-5758.
- 14. Wang, J.; Chen, X.; Guo, B.; Yang, X.; Zhou, Y.; Zhu, X.; Zhang, K.; Fan, Y.; Tu, C.; Zhang, X. A serum protein adsorption profile on BCP ceramics and influence of the elevated adsorption of adhesive proteins on the behaviour of MSCs. *J Mater Chem B.* 2018, 6, 7383-7395.
- Wang, Z.; Lin, S. The impact of low-surface-energy functional groups on oil fouling resistance in membrane distillation. J Membr Sci. 2017, 527, 68-77.
- Rosales, J. I.; Marshall, G. W.; Marshall, S. J.; Watanabe, L. G.;
  Toledano, M.; Cabrerizo, M. A.; Osorio, R. Acid-etching and hydration influence on dentin roughness and wettability. *J Dent Res.* 1999, 78, 1554-1559.
- Lu, Z.; Wu, Y.; Cong, Z.; Qian, Y.; Wu, X.; Shao, N.; Qiao, Z.; Zhang, H.; She, Y.; Chen, K.; Xiang, H.; Sun, B.; Yu, Q.; Yuan, Y.; Lin, H.; Zhu, M.; Liu, R. Effective and biocompatible antibacterial surfaces via facile synthesis and surface modification of peptide polymers. *Bioact Mater*. 2021, 6, 4531-4541.
- 18. Zhao, G.; Schwartz, Z.; Wieland, M.; Rupp, F.; Geis-Gerstorfer, J.; Cochran, D. L.; Boyan, B. D. High surface energy enhances cell response to titanium substrate microstructure. *J Biomed Mater Res A.* **2005**, *74*, 49-58.

#### Nanotopography and surface energy regulate osteogenesis

- Feng, B.; Weng, J.; Yang, B. C.; Qu, S. X.; Zhang, X. D. Characterization of surface oxide films on titanium and adhesion of osteoblast. *Biomaterials*. 2003, 24, 4663-4670.
- Nakamura, M.; Hori, N.; Ando, H.; Namba, S.; Toyama, T.; Nishimiya, N.; Yamashita, K. Surface free energy predominates in cell adhesion to hydroxyapatite through wettability. *Mater Sci Eng C Mater Biol Appl.* 2016. 62, 283-292.
- Razafiarison, T.; Holenstein, C. N.; Stauber, T.; Jovic, M.; Vertudes, E.; Loparic, M.; Kawecki, M.; Bernard, L.; Silvan, U.; Snedeker, J. G. Biomaterial surface energy-driven ligand assembly strongly regulates stem cell mechanosensitivity and fate on very soft substrates. *Proc Natl Acad Sci U S A.* 2018, 115, 4631-4636.
- 22. Faghihi, S.; Azari, F.; Szpunar, J. A.; Vali, H.; Tabrizian, M. Titanium crystal orientation as a tool for the improved and regulated cell attachment. *J Biomed Mater Res A.* **2009**, *91*, 656-662.
- Dykman, L.; Khlebtsov, N. Gold nanoparticles in biomedical applications: recent advances and perspectives. *Chem Soc Rev.* 2012, 41, 2256-2282.
- Huang, D.; Liao, F.; Molesa, S.; Redinger, D.; Subramanian, V. Plasticcompatible low resistance printable gold nanoparticle conductors for flexible electronics. *J Electrochem Soc.* 2003, 150, G412.
- Khan, I.; Saeed, K.; Khan, I. Nanoparticles: Properties, applications and toxicities. *Arab J Chem.* 2019, 12, 908-931.
- Tiwari, P. M.; Vig, K.; Dennis, V. A.; Singh, S. R. Functionalized gold nanoparticles and their biomedical applications. *Nanomaterials (Basel)*. 2011, 1, 31-63.
- Yáñez-Sedeño, P.; Pingarrón, J. M. Gold nanoparticle-based electrochemical biosensors. Anal Bioanal Chem. 2005, 382, 884-886.
- Sousa, L. M.; Vilarinho, L. M.; Ribeiro, G. H.; Bogado, A. L.; Dinelli, L. R. An electronic device based on gold nanoparticles and tetraruthenated porphyrin as an electrochemical sensor for catechol. *R Soc Open Sci.* 2017, 4, 170675.
- 29. Holec, D.; Dumitraschkewitz, P.; Vollath, D.; Fischer, F. D. Surface energy of au nanoparticles depending on their size and shape. *Nanomaterials (Basel).* **2020**, *10*, 484.
- Grzelczak, M.; Pérez-Juste, J.; Mulvaney, P.; Liz-Marzán, L. M. Shape control in gold nanoparticle synthesis. *Chem Soc Rev.* 2008, 37, 1783-1791.
- Zhang, Q.; Large, N.; Nordlander, P.; Wang, H. Porous Au nanoparticles with tunable plasmon resonances and intense field enhancements for single-particle SERS. J Phys Chem Lett. 2014, 5, 370-374.
- 32. Zhang, Q.; Large, N.; Wang, H. Gold nanoparticles with tipped surface structures as substrates for single-particle surface-enhanced Raman spectroscopy: concave nanocubes, nanotrisoctahedra, and nanostars. *ACS Appl Mater Interfaces.* **2014**, *6*, 17255-17267.
- 33. Zhang, Q.; Zhou, Y.; Villarreal, E.; Lin, Y.; Zou, S.; Wang, H. Faceted Gold Nanorods: Nanocuboids, Convex Nanocuboids, and Concave Nanocuboids. *Nano Lett.* **2015**, *15*, 4161-4169.
- 34. Petryayeva, E.; Krull, U. J. Localized surface plasmon resonance: nanostructures, bioassays and biosensing--a review. *Anal Chim Acta.* **2011**, *706*, 8-24.
- Orendorff, C. J.; Sau, T. K.; Murphy, C. J. Shape-dependent plasmonresonant gold nanoparticles. Small. 2006, 2, 636-639.
- Malmsten, M. Formation of adsorbed protein layers. J Colloid Interface Sci. 1998, 207, 186-199.
- Wertz, C. F.; Santore, M. M. Effect of surface hydrophobicity on adsorption and relaxation kinetics of albumin and fibrinogen: single-

- species and competitive behavior. Langmuir. 2001, 17, 3006-3016.
- 38. Latour, R. A. Biomaterials: protein-surface interactions. In *Encyclopedia of Biomaterials and Biomedical Engineering*, Wnek, G.; Bowlin, G., eds.; CRC Press: **2008**; pp 270-284.
- Deng, Z. J.; Mortimer, G.; Schiller, T.; Musumeci, A.; Martin, D.; Minchin, R. F. Differential plasma protein binding to metal oxide nanoparticles. *Nanotechnology*. 2009, 20, 455101.
- Zernik, J.; Twarog, K.; Upholt, W. B. Regulation of alkaline phosphatase and alpha 2(I) procollagen synthesis during early intramembranous bone formation in the rat mandible. *Differentiation*. 1990, 44, 207-215.
- Igarashi, M.; Kamiya, N.; Hasegawa, M.; Kasuya, T.; Takahashi, T.;
  Takagi, M. Inductive effects of dexamethasone on the gene expression of Cbfa1, Osterix and bone matrix proteins during differentiation of cultured primary rat osteoblasts. *J Mol Histol.* 2004, *35*, 3-10.
- Li, Y.; Kim, J. H.; Choi, E. H.; Han, I. Promotion of osteogenic differentiation by non-thermal biocompatible plasma treated chitosan scaffold. Sci Rep. 2019, 9, 3712.
- 43. Lim, E. K.; Keem, J. O.; Yun, H. S.; Jung, J.; Chung, B. H. Smart nanoprobes for the detection of alkaline phosphatase activity during osteoblast differentiation. *Chem Commun (Camb)*. **2015**, *51*, 3270-3272.
- Yuan, J.; Maturavongsadit, P.; Metavarayuth, K.; Luckanagul, J. A.;
  Wang, Q. Enhanced bone defect repair by polymeric substitute fillers of multiarm polyethylene glycol-crosslinked hyaluronic acid hydrogels. *Macromol Biosci.* 2019, 19, e1900021.
- Yang, Y. K.; Ogando, C. R.; Wang See, C.; Chang, T. Y.; Barabino,
  G. A. Changes in phenotype and differentiation potential of human mesenchymal stem cells aging in vitro. Stem Cell Res Ther. 2018, 9, 131.
- 46. Neuhuber, B.; Swanger, S. A.; Howard, L.; Mackay, A.; Fischer, I. Effects of plating density and culture time on bone marrow stromal cell characteristics. *Exp Hematol.* **2008**, *36*, 1176-1185.
- 47. Parhi, P.; Golas, A.; Vogler, E. A. Role of proteins and water in the initial attachment of mammalian cells to biomedical surfaces: A Review. *J Adhes Sci Technol.* **2010**, *24*, 853-888.
- Lim, J. Y.; Liu, X.; Vogler, E. A.; Donahue, H. J. Systematic variation in osteoblast adhesion and phenotype with substratum surface characteristics. *J Biomed Mater Res A.* 2004, 68, 504-512.
- Liu, X.; Lim, J. Y.; Donahue, H. J.; Dhurjati, R.; Mastro, A. M.; Vogler, E. A. Influence of substratum surface chemistry/energy and topography on the human fetal osteoblastic cell line hFOB 1.19: Phenotypic and genotypic responses observed in vitro. *Biomaterials*. 2007, 28, 4535-4550.
- Baier, R. E.; Meyer, A. E.; Natiella, J. R.; Natiella, R. R.; Carter, J. M. Surface properties determine bioadhesive outcomes: methods and results. J Biomed Mater Res. 1984, 18, 337-355.
- 51. Groth, T.; Altankov, G. Studies on cell-biomaterial interaction: role of tyrosine phosphorylation during fibroblast spreading on surfaces varying in wettability. *Biomaterials*. **1996**, *17*, 1227-1234.
- Schakenraad, J. M.; Busscher, H. J.; Wildevuur, C. R.; Arends, J. Thermodynamic aspects of cell spreading on solid substrata. *Cell Biophys.* 1988, 13, 75-91.
- 53. Tamada, Y.; Ikada, Y. Fibroblast growth on polymer surfaces and biosynthesis of collagen. *J Biomed Mater Res.* **1994**, *28*, 783-789.

Received: April 5, 2021 Revised: June 7, 2021 Accepted: June 9, 2021 Available online: June 28, 2021